International Journal of Heat and Fluid Flow 30 (2009) 549–560

Contents lists available at ScienceDirect

International Journal of Heat and Fluid Flow

journal homepage: www.elsevier.com/locate/ijhff

URANS of flow and endwall heat transfer in a pinned passage relevant to gas-turbine blade cooling

G. Delibra[a], D. Borello[a,*], K. Hanjalić[a,b], F. Rispoli[a]

[a] Dipartimento di Meccanica e Aeronautica, 'Sapienza' Università di Roma, Via Eudossiana 18, 00187 Roma, Italy
[b] Dept. of Multi-scale Physics, Delft University of Technology, The Netherlands

ARTICLE INFO

Article history:
Received 7 October 2008
Received in revised form 6 March 2009
Accepted 10 March 2009
Available online 5 May 2009

Keywords:
URANS
LES
Unsteadiness
Heat transfer
Pinned passages
Gas-turbine blade internal cooling

ABSTRACT

This paper presents some results of URANS study of flow and heat transfer in a matrix of wall-bounded 8×8 round pins, mimicking internal cooling passage of gas-turbine blades. The focus is on flow unsteadiness, its role in heat transfer and the capabilities of RANS models to reproduce these features in a set-up of industrial relevance. The results for two Reynolds numbers, 10 000 and 30 000, are compared with the available experiments and LES. It is shown that the elliptic-relaxation eddy-viscosity model, ζ-f captures vortex shedding and the consequent gross effects on the flow development. However, a closer look at flow details reveals discrepancies, especially around the first three pin rows, where the unsteadiness reproduced by URANS shows much weaker amplitudes as compared with LES. Only further downstream the succession of forcing from a series of pins produced unsteadiness akin to those captured by LES. The comparison suggests that smaller structures undetected by URANS need to be resolved to capture properly the separation and wake characteristics of each row. At Re = 10 000, the average endwall Nusselt number agrees well with the LES, both being about 20% lower than in the experiment. For Re = 30 000 the URANS Nusselt is within 10% of the experimental value.

1. Introduction

Design and optimization of internal cooling of gas-turbine blades rely heavily on Computational Fluid Dynamics (CFD) and conventional RANS models. However, the real configurations are usually geometrically and physically complex, involving three-dimensionality, unsteadiness, system rotation, laminar-to-turbulent and reverse transition, which all still pose challenge to common RANS models that are found in commercial CFD packages. Contradictory findings have been reported in the literature on the successes (e.g. Borello et al., 2007; Durbin, 1995) and failures (e.g. Rodi et al., 1997) of various RANS models in reproducing the main flow features of industrially relevant quantities, especially in more complex flows. The judgment depends, however, on the criteria of what quality of results can be considered as satisfactory (which parameters are considered, what is the required degree of accuracy, how reliable are the reference data for benchmarking), but also on the complexity of the problem considered, the level and sophistication of the adopted RANS model, numerical schemes and computational grid.

It is generally recognised that a URANS model that performs well in steady flows, can return credible predictions of unsteady phenomena only if the unsteadiness is imposed externally and at time scales which are much larger than the characteristic turbulence scale. The scale separation criterion is seldom satisfied in flows with internal unsteadiness originating from inherent flow instabilities due to flow separation, unstable stratification or external body force. Nevertheless, good agreement of URANS results with the experimental and LES data have been reported e.g. in flows dominated by self-generated semi-deterministic forcing in thermal convection in stagnant fluids heated from below, where the stochastic turbulence was found to behave much as a passive scalar (e.g. Hanjalić and Kenjereš, 2001, 2006). Capturing the dynamics of vortex shedding behind bluff bodies with URANS and the consequences on flow and heat transfer is, however, less certain. In principle, a URANS model can capture unsteady vortex shedding behind bluff bodies away from other walls (acceptably accurate frequency, wake size and shape), such as in flow around a long free cylinder in a cross stream (e.g. Rodi, 1993). However, their breakup and subsequent interaction with the stochastic turbulence generated in the accompanied shear layers, especially if the incoming flow is non-turbulent – thus involving separation-induced transition, is a challenge for common URANS. The eddy-viscosity obtained from a RANS model would need to be substantially reduced to make the model more sensitive to instabilities of different characteristic wavelengths, and this is the direction pursued by various hybrid RANS–LES approaches (Hanjalić, 2005; Frolich and von Terzi, 2008).

* Corresponding author. Tel.: +39 06 44585233; fax: +39 06 4881759.
E-mail address: borello@dma.ing.uniroma1.it (D. Borello).

0142-727X/$ - see front matter © 2009 Elsevier Inc. All rights reserved.
doi:10.1016/j.ijheatfluidflow.2009.03.015

The challenge to URANS becomes still larger in flows through arrays or matrices of closely spaced multiple bluff bodies bounded by surrounding walls, as for example found in tube-in-shell heat exchanges, or in the here considered configuration of staggered cylindrical pins bounded by endwalls. In such configuration the pins and tubes, and in particular the bounding walls – if spaced close to each other – suppress instabilities and in some cases the common URANS models can fail to capture any unsteadiness contrary to experimental or LES evidence. In view of the fact that (U)RANS continue to serve as the mainstay of industrial CFD despite its known shortcomings, the question of a broader interest is how important it is to reproduce the internal flow unsteadiness in predicting the common engineering parameters such as pressure drop, drag and heat transfer. And, if so, what are the basic deficiencies and can they be located and eliminated by using more advanced models or by some plausible model modifications. These issues constitute the main focus of the present work.

In an ongoing project we have studied the performance of several RANS models in parallel with LES and hybrid RANS/LES in a generic three-dimensional turbulent flow with inherent unsteadiness generated by vortex shedding from multiple short cylindrical pins bounded by plane heated walls. Similar configurations have been extensively studied by experimentalists, see e.g. the studies of Metzger et al. (1986). In contrast, only few computational studies appeared in the literature in the recent years and most of them are related to simplified configurations (periodic segments) involving bundles of relatively long tubes as found in heat exchangers, e.g. Watterson et al. (1999), Benhamadouche and Laurence (2003). The flow configuration considered here is the one studied experimentally by Ames et al. (2005), Ames and Dvorak (2006), Ames et al. (2007), which provided measurements of mean flow and some turbulence parameters at Reynolds number or 3000, 10 000 and 30 000, which can be used for validating the computational results. The relatively compact pin arrangement and especially the endwalls distanced only two pin diameters are expected to suppress instabilities as compared with pin matrices with larger spacing and endwall distances. The aim is to test in more complex flows relatively simple, industry-appealing, robust (U)RANS models that have already shown good performance in predicting steady wall-bounded flows and heat transfer in canonical configurations as well as in flows of industrial relevance. Specifically, the target is to identify the receptivity and the dynamic response of the model to forcing induced by a sequence of vortex shedding at different Re numbers, and the model capability to capture major flow features in a reference flow with a view to possible application to real blade cooling configurations.

This study is not a straightforward validation of the adopted RANS model, or its comparison with other models, but rather an attempt to identify its potential or the lack of it to reproduce those flow and turbulence features that are most influential in predicting the endwall heat transfer. Among several issues, we consider the following:

- The receptivity of the RANS model to natural forcing due to vortex shedding from arrays of multiple bluff bodies bounded by solid walls.
- The importance of flow unsteadiness in reproducing the long-term average flow and heat transfer parameters.

The latter issue can be reformulated as whether it is sufficient to capture the well-organised (semi) deterministic vortex shedding which are usually reproduced by more advanced closures in the URANS mode, or does one need to resolve a significant portion of the (large-scale) turbulence spectrum by using LES, or at least a hybrid RANS/LES?

To this purpose we have considered the ζ-f elliptic-relaxation model, which was shown to perform well in a number of generic flows (Hanjalić et al., 2004, 2005) as well as in industrial flows (Tatschl et al.,2006; Krajnović et al., 2008; Basara, 2009). In parallel, we considered LES of the same flow (using a moderately dense and a fine grid) to serve as a reference for the lower Reynolds number (Delibra et al., 2008). The future target is a hybridisation of the ζ-f model with LES as well as some options of T-RANS ("seamless") approach which use only a simple conventional integration-to-wall (ItW) RANS model (such as ζ-f), but sensitized to recover a portion of the turbulence spectrum (Borello et al., 2009).

Not all RANS models are equally sensitive to inherent flow instabilities: second-moment closures should be more receptive because of their capabilities to model the stress anisotropy, which seems essential for three-dimensionalizing the usually two-dimensional initial instabilities, as well as for initiating the laminar-to-turbulent transition in wall flows. However, at present we confine our attention to the ζ-f model because it is simple and robust and yet superior to the standard two equations eddy-viscosity models, especially in reproducing the wall effects. It mimics at least some stress anisotropy by solving a separate equation for $\zeta = v^2/k$, where v^2 comes close to wall-normal turbulent stress component in wall vicinity and k is the turbulent kinetic energy This is especially important if wall friction and heat transfer are the primary focus, as is the case in the present work and in most industrial computations.

Admittedly, despite substantial physical enhancement by the introduction of elliptic-relaxation, the ζ-f model here considered, just as its predecessor, the Durbin's (1991) v^2-f model, is a linear eddy-viscosity model, which cannot be expect to reproduce accurately the three-dimensional effects. Further research by using more advanced models, preferably at the second-moment closure level, could shed more light on the receptivity of URANS to inherent unsteadiness. However, we believe that the present study, although limited to a particular linear RANS model, offers already some interesting and reasonably general conclusions of relevance to industrial CFD. Using the reference experimental and LES data, and structure morphology educed from LES, an attempt is made to identify the major modelling prerequisites for reproducing the salient features of flow, turbulence and the dominant vortical structures, which are relevant for heat transfer.

2. Flow configuration and computational details

The flow configuration considered in the experiments of Ames and co-workers (2005, 2006, 2007) mimics internal cooling of a gas-turbine blade. It is essentially a flow in a plane channel in which a matrix of 8×8 round pins, connecting the channel "endwalls", is placed in a staggered arrangement. The pin spacing was $2.5D$ in the lateral and $5D$ in the streamwise direction (where $D = 2.54$ cm denotes the pin diameter), thus making the spacing between pin rows in both directions $2.5D$, Fig. 1. The channel height (pin length) is $2D$. The centre of the first pin row is located $7.5D$ downstream from the nozzle, thus allowing for some development of boundary layers on endwalls. The inflow turbulence in the experiment was claimed to be about 1.4%. The channel exit (followed by a 90° bend) is located $7.5D$ downstream from the centre of the last, eighth pin row. The air flowing through the channel should remove excessive heat from the "blade" walls through the pins. Thus, the main interest is in heat transfer on the endwalls. We considered two higher Reynolds number of 10 000 and 30 000, based on D and the averaged velocity in the minimum passage area between the pins V_{max}.

One of the uncertainties in mimicking the experiment is the proper specification of inflow conditions. The fluid enters the

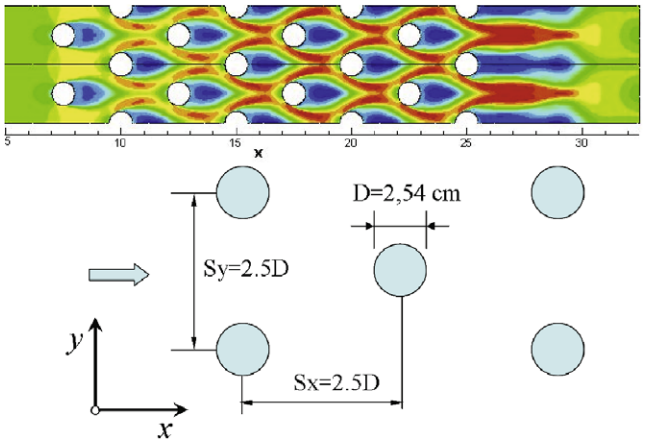

Fig. 1. Flow configuration and a typical flow pattern with contours of mean velocity at midplane (Re = 10 000).

channel through a nozzle. In order to diminish as much as possible the effect of the inflow and outflow conditions, we considered in all computations the complete channel length, but only a segment in the spanwise direction using periodic conditions on the domain side boundaries. For Re = 10 000, this segment contained only one pin row (Fig. 1). For Re = 30 000 the spanwise width of the solution domain was doubled in order to eliminate possible side cutting of the flow structures. The computational mesh consisted of 1.3 and 2.5 million cells, for the lower and higher Re number respectively. The meshes were clustered around pins and endwalls, with y^+ values of the wall-nearest cell centres less than 2 in most of the domain for Re = 10 000 and less than 4 for Re = 30 000, except is small local areas around flow separation and reattachment.

The computations were performed using the in house T-FlowS unstructured parallel finite-volume code (Ničeno and Hanjalić, 2005). The incompressible Navier Stokes equation system is solved using the Conjugate Gradient solver with the SIMPLE algorithm for velocity–pressure coupling. As convective schemes, SMART and CDS are used for URANS and LES respectively for all the variables, with Crank Nicholson time integration scheme for the lower Re and fully implicit time integration scheme for the higher Re. The non-dimensional time steps ($\Delta t^* = \Delta t U_{ref}/D$) have been set to 0.004 for Re = 10 000 and 0.007 for Re = 30 000. This allowed to have a CFL < 1 everywhere. The time steps used to obtain fully convergent results are reported in Table 1. In all the simulations the convergence threshold parameters was set equal to 10^{-8} for the field variables in the iterative cycle for resolving each time step. The tolerance value for the SIMPLE algorithm was set to 10^{-6}.

3. The RANS model

The ζ-f model (Hanjalić et al., 2004, 2005) is an eddy-viscosity model based on Durbin's (1991) elliptic-relaxation concept, which solves a transport equation for $\zeta = v^2/k$ instead of the equation for v^2, in conjunction with the ItW version of the k and ε equations, and an elliptic-relaxation function (here based on a quasi-linear pressure–strain model),

$$\frac{D\zeta}{Dt} = f - \frac{\zeta}{k}P_k + \frac{\partial}{\partial x_j}\left[(\nu + \nu_t)\frac{\partial \zeta}{\partial x_j}\right] \tag{1}$$

$$L^2\nabla^2 f - f = \frac{1}{\tau}\left(c_1 + C_2\frac{P_k}{\varepsilon}\right)\left(\zeta - \frac{2}{3}\right) \tag{2}$$

$$\frac{Dk}{Dt} = P_k - \varepsilon + \frac{\partial}{\partial x_k}\left[(\nu + \nu_t)\frac{\partial k}{\partial x_k}\right] \tag{3}$$

$$\frac{D\varepsilon}{Dt} = \frac{C_{\varepsilon_1}P_k - C_{\varepsilon_2}\varepsilon}{\tau} + \frac{\partial}{\partial x_k}\left[\left(\nu + \frac{\nu_t}{\sigma_\varepsilon}\right)\frac{\partial \varepsilon}{\partial x_k}\right] \tag{4}$$

where τ and L are the time and length scale respectively taking the conventional values $\tau = k/\varepsilon$ and $L = k^{3/2}/\varepsilon$ away from a solid wall, but with Kolmogorov scales bounding their minimum values, i.e.

$$\tau = \max\left[\min\left(\frac{k}{\varepsilon}, \frac{0.6}{\zeta c_\mu\sqrt{6S^2}}\right), C_\tau\left(\frac{\nu}{\varepsilon}\right)^{1/2}\right] \tag{5}$$

$$L = C_L\max\left[\min\left(\frac{k^{3/2}}{\varepsilon}, \frac{k^{1/2}}{\zeta c_\mu\sqrt{6S^2}}\right), C_\eta\left(\frac{\nu^3}{\varepsilon}\right)^{1/4}\right] \tag{6}$$

Eqs. (5) and (6) contain also Durbin's realisability constraints that control the excessive growth of τ and L.

The eddy-viscosity is defined as $\nu_t = c_\mu\zeta k\tau$, where $c_\mu = 0.22$ corresponds to the conventional $C_\mu = 0.09$ in an equilibrium wall shear layer where $\zeta \approx 0.4$. Because of a more convenient formulation of the equation for ζ and especially of the wall boundary condition for the elliptic-function $f_w = -2\nu\zeta/y^2$, this model is more robust and less sensitive to non-uniformities and clustering of the computational grid than the original v^2-f model. Alternatively, one can solve Eq. (2) for a "homogeneous" function $\tilde{f}$ with zero wall boundary conditions $\tilde{f}_w = 0$, and then obtain $f = \tilde{f} - 2\nu(\partial\zeta^{1/2}/\partial x_n)^2$ (in analogy with Jones–Launder equation for homogeneous dissipation). Other coefficients, originating from the standard k–ε, Re-stress and v^2-f models take the values: $c_1 = C_1 - 1 = 0.8$, $C_2 = 0.6$, $C_{\varepsilon 1} = 1.44$, $C_{\varepsilon 2} = 1.92$, $\sigma_\varepsilon = 1.3$, $C_L = 0.36$, $C_\tau = 6.0$, $C_\eta = 85.0$. The model was earlier tested in a series of generic cases, including of flow and heat transfer in a plane channel, behind a backward facing step and in a round impinging jet, all showing satisfactory agreement with the available experiments and direct numerical simulations (Hanjalić et al., 2004, 2005). It was also applied to a number of complex internal and external industrial flows (Basara, 2009; Tatschl et al., 2006; Krajnović et al., 2008).

The energy equation is resolved in the form of temperature. The turbulent fluxes are modeled by using the standard (isotropic) eddy-diffusivity ν_t/Pr_T model in which the turbulent Prandtl number Pr_T is evaluated from the Kays and Crawford (1993) formula.

4. Results and discussion

In order to get an overall impression of the flow configuration and anticipated flow pattern and phenomena, Fig. 1 shows the pin arrangement together with the long-term averaged velocity field for Re = 10 000 in the midplane between the endwalls. Because the incoming flow is uniform with low free-stream turbulence, the fully turbulent periodic regime develops only at around fourth to seventh row, though no fully repeatable pattern is ever established. The last row generates a very elongated wake in the remaining unobstructed part of the channel, which exerts some visible upstream effects. While this average flow patters does not differ much from those inferred from LES and experiments (see

Table 1
Number of time steps.

LES simulation Re = 10 000	ζ-f simulation Re = 10 000	ζ-f simulation Re = 30 000
50 000 – heating imposed after 30 000 time step	40 000 – heating imposed after 20 000 time step	22 000 – heating imposed after 14 000 time step

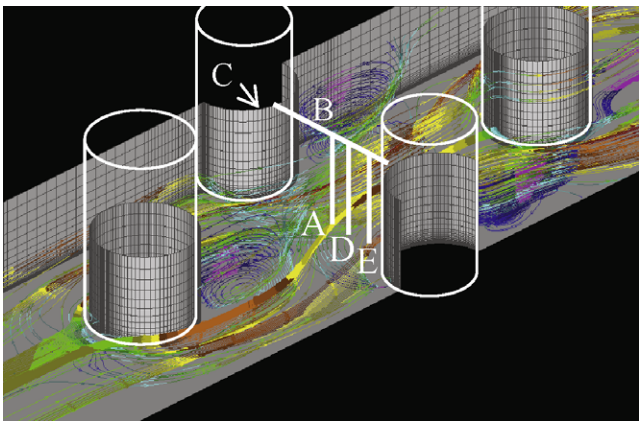

Fig. 2. A segment of the solution domain, and a snapshot of URANS instantaneous streamlines around the first four rows; A, B, C, D and E indicate lines along which the computational results are compared with experiments.

discussion on heat transfer below), the latter undoubtedly indicates that the flow is unsteady in the whole domain starting with the first pin row. Vortices shed from the first two rows impose the characteristic frequency of the basic unsteady mode. The URANS ζ-f captures periodicity of vortex shedding already behind the first row, though with much smaller amplitudes than detected in the experiments and LES. The computed Strouhal numbers for the first pin, St = 0.244 for Re = 10 000 and 0.238 for Re = 30 000, are very close to the measured values 0.234 and 0.209. A typical instantaneous streamline pattern captured by URANS around the first four pins is illustrated by a snapshot in Fig. 2. The URANS mesh resolution in the direction normal to the endwall (for the lower Re) is also shown. The characteristic horse-shoe vortex in front of the first pin close to the endwall, is also qualitatively well reproduced.

As noted above the incoming flow is non-turbulent. As illustrated by the evolution of the turbulence Reynolds number $\mathrm{Re}_t = k^2/(\nu\varepsilon)$ in Fig. 3, the URANS predicts correctly that turbulence develops first in the wakes of the first pin rows, which then enhances further turbulence production in the impingement zones and around the pins in the subsequent rows. However, a visualizations of vortical structures captured by LES reveals a broad spectrum of structure sizes in the whole flow domain, as illustrated by the pressure Laplasian ($\nabla^2 p$) in Fig. 4. As expected, at both Reynolds number, the URANS captures only the relatively smooth pattern of the initially almost two-dimensional vortices generate behind the pins. In view of the obvious strong smoothing, the success of URANS in predicting flow parameters of industrial relevance will depend on the importance of the unresolved structures. We show first some mean flow parameters and analyze subsequently in more details the unsteadiness reproduced by URANS and its role in the formation of the mean flow velocity and temperature fields, compared with the LES results.

4.1. Mean flow properties

We begin by discussing the mean velocity profiles in some characteristic planes, compared with LES and experiments. It is noted that the velocity was measured only in the cross-sections between the pins (at 90°) at the pin mid-heights (line B, Fig. 2), normal to the bottom endwall in the middle between the pins (line A), and these measurements are available only for the four rows, the first three and the fifth one. For Re = 30 000 additional velocity profiles are available (Dvorak, 2004) for the cutlines between the central vertical axis between the pins and the pin surface at 90° for row 3, denoted in Fig. 2 as D and E lines.

A selection of the URANS computations for the two Re numbers for the first, second, third and fifth row is presented in Figs. 5–7, together with the measured data and LES results (the latter only

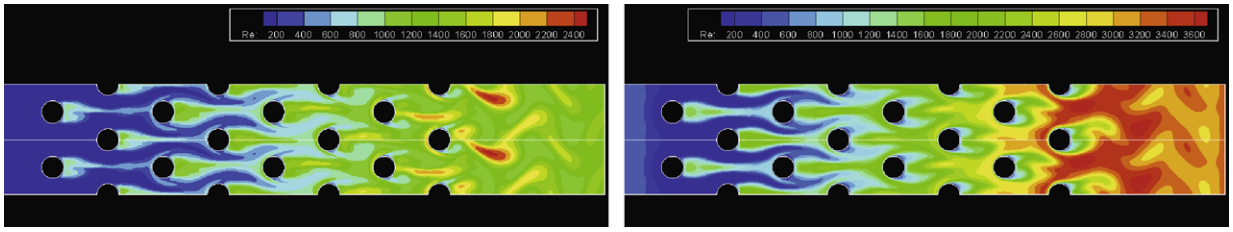

Fig. 3. A snapshot of instantaneous contours of the turbulence Reynolds number, $\mathrm{Re}_t = k^2/(\nu\varepsilon)$, for Re = 10 000, computed by URANS ζ-f. In a near-wall plane at 5% of the pin height (left) and in the midplane (right).

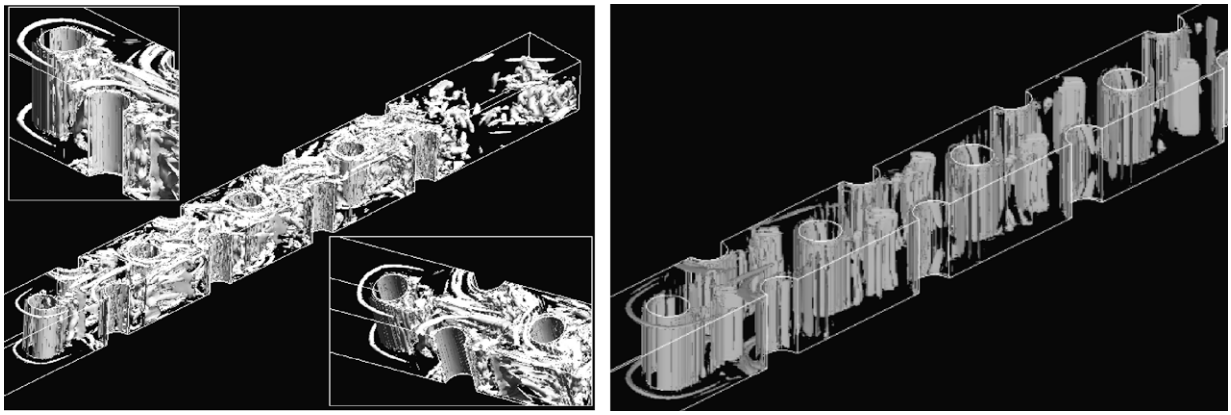

Fig. 4. Vortical structures identified by the instantaneous $\nabla^2 p = 7$ for Re = 10 000. Left: LES; right: URANS ζ-f.

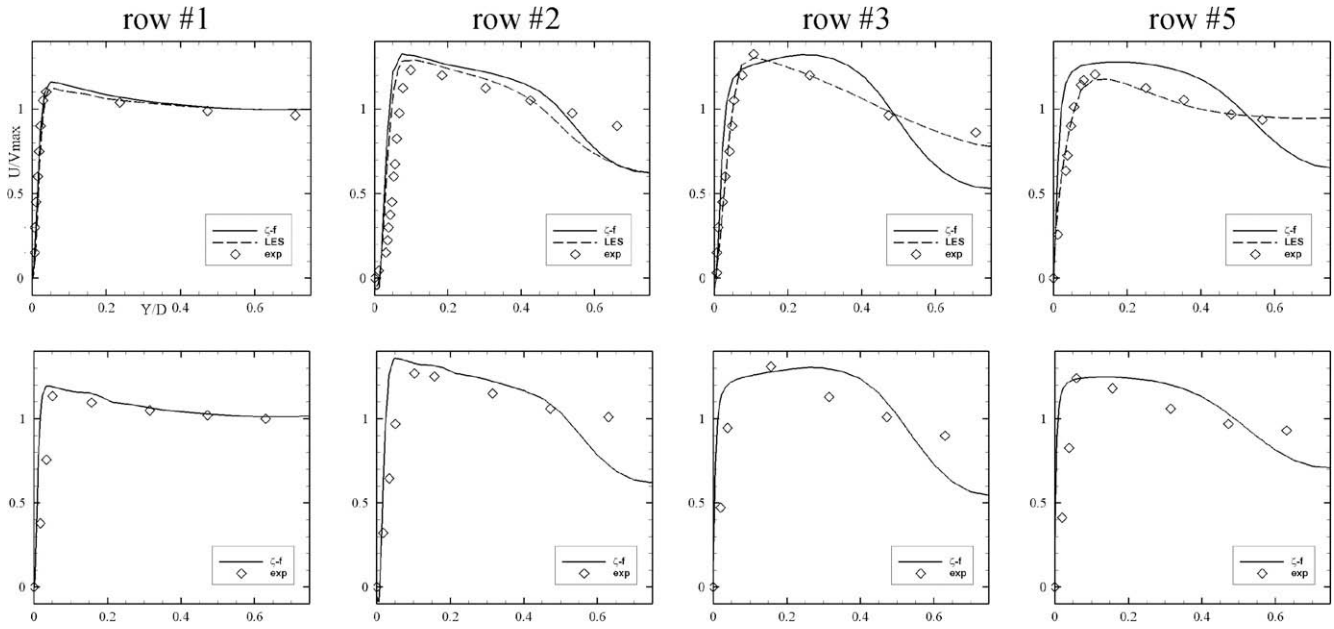

Fig. 5. Comparison of mean velocity profiles obtained by URANS ζ-f, LES and experiments (Ames et al., 2005) in horizontal midplane between neighbouring pins, lines B (only half profiles are shown). Top: Re = 10 000. Bottom: Re = 30 000.

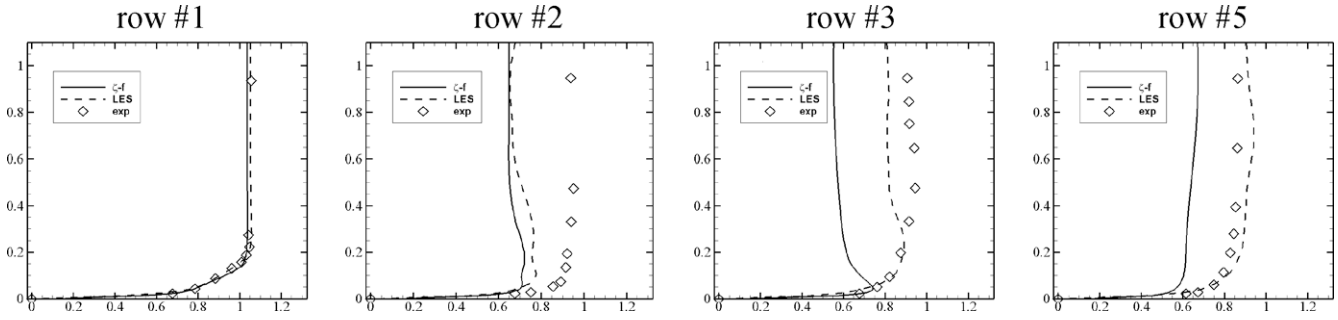

Fig. 6. Comparison of mean velocity profiles obtained by URANS ζ-f, LES and experiments (Ames et al., 2005) in the vertical midplanes between the two pin rows, lines A. Re = 10 000.

for Re = 10 000). We note first that the quality of results is very similar for the two Re numbers. Despite uncertainties regarding the inflow conditions, the URANS reproduced the mean flow velocity at 90° of the first pin row in excellent agreement with both the experiments and LES, as shown in Fig. 5. Admittedly, as noted above, the flow here is almost laminar – with a small uniform inflow turbulence level, possibly being slightly enhanced in the thin boundary layers developing around the pins, as indicated in Fig. 3 by the contours and shades of turbulent Reynolds number. Already at the second and the subsequent rows, the URANS predictions show visible discrepancies from the experimental results, primarily in the central region away from the pins, as best illustrated in Fig. 6. Interestingly, LES came to close agreement with experiments for all rows except for row 2 where URANS and LES agree with each other but not with the experiments. Along line A (normal to the endwall) both computational approaches predict a kind of mild wall-jet-like profiles with a velocity maximum close to the wall, whereas experiments show a monotonic standard wall boundary-layer type profiles. The computed lower velocities in the outer regions indicate that a part of fluid is escaping elsewhere, suggesting a strong three-dimensionality effect. This is confirmed by a comparison of the profiles along the cutlines D and E normal to the endwall between the third row pins at different distance from pin axis, Fig. 7. Contrary to possible inference from Fig. 6, it evident that the total computed mass flow rates agrees well with the experiment, but at some cutlines the computed velocity is higher and at some lower than measured. Because (apart from the second row) LES captures well the velocity profiles in all cross-sections, we suspect that the origin of the URANS failure in this central flow region is in the limitation of the here used linear eddy-viscosity model to capture accurately the flow three-dimensionality.

Another cause could be traced in inadequate location of transition from the incoming non-turbulent flow washing the first pin to fully turbulent regime further downstream. The flow separation from the first pin is obviously laminar and the transition to turbulence behind the first pin is induced by separation and recirculation within the shed vortices. In contrast to the URANS computations, which show very similar flow pattern and turbulence level around the second pin row, the LES generated vortical structures in Fig. 4 shows that the second pins are affected by vortical structures shed from the first pins and related disturbances propagated from their wakes. This enhances a faster developing of the boundary layer on the second and subsequent pins, affecting also the flow in the central passages. In brief, the disagreement of

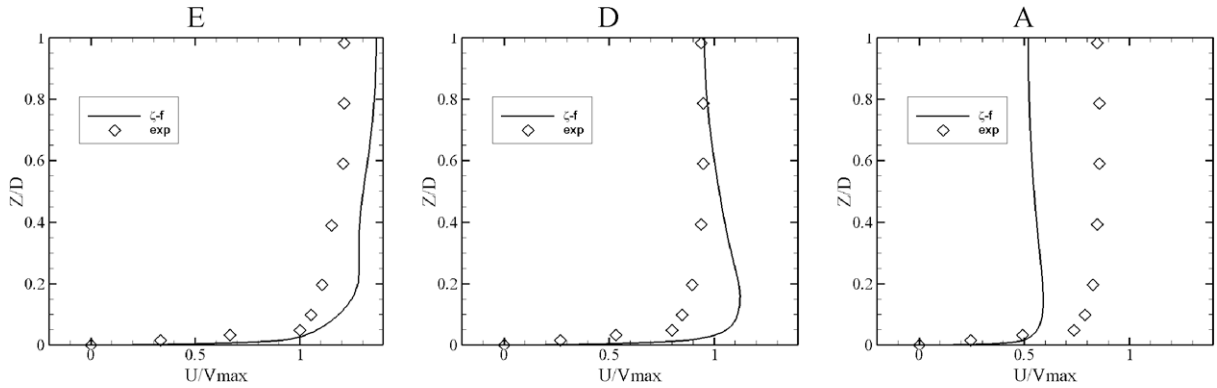

Fig. 7. Comparison of mean velocity profiles obtained by URANS ζ-f and experiments (Dvorak, 2004) in the vertical midplane between the two pins along lines E, D and A (Fig. 2), row 3, Re = 30 000.

URANS velocity profiles as from the second row seems to be the consequence of inadequate predictions of the wake length, the strength of recirculation as well as the level of turbulence.

This is further confirmed by the pressure coefficient, shown in Fig. 8, together with experimental data and LES results. It is remarkable that on the front impingement side, the URANS returns good pressure coefficient for almost all rows. This can be attributed to the scale-realizability constraint, Eqs. (5) and (6), which improve predictions in stagnation region. The shortcomings of URANS appear in predicting the accurate position of the flow separation and especially in capturing properly the near-wake length and the intensity of recirculation. For most pin rows, LES performs superior.

However, there are some odd results which we cannot explain at present. For example, for the fifth row at Re = 10 000, the URANS ζ-f agrees almost perfect with experiments, whereas coarse LES shows a visible disagreement. This finding is not in conflict with the excellent LES predictions of the mean velocity in the cross-section between the pins for all rows, since this agreement does not guarantee the accurate predictions in the pin wakes. It is expected that the wake structure and intensity will depend on the turbulence generated in and around the separation. As noted earlier, in contrast to the bulk unsteadiness, the URANS did not reproduce well the flow instability and the experimentally detected notable oscillations – an intermittent character – of the separation location, which probably reflects in inadequate prediction of the wakes.

We return briefly to the cross-section between the pins and consider the velocity distribution close to the pin surface. Fig. 9 shows a comparison of URANS and LES computations with experiments for the first pin row at the lower Re. The results are normalised with the average maximum velocity $V_{max.}$ The URANS ζ-f and LES show very good agreement in between, and both are relatively close to the measured values. It is recalled that velocity was measured with a hot wire, which is prone to various errors when used very close to a solid wall.

A better judgement could be made when velocity is normalised with wall scales, the friction velocity and viscosity. A value of the friction factor at this point (at 90°) has been quoted in the experiment (evaluated by fitting the velocity profile in the buffer region, for $4 < y+ < 10$ to Spalding equation for the universal velocity distribution), but neither URANS nor LES could reproduced it for any of the considered Re numbers. Ames and Dvorak (2006) reported the separation on the first pin to occur at 82–83°. (obtained from the pressure coefficient and Thwaite's formula) for the two Re numbers here considered, whereas the present URANS computations give values of 85° and 87°. respectively. Thus, both the experimental

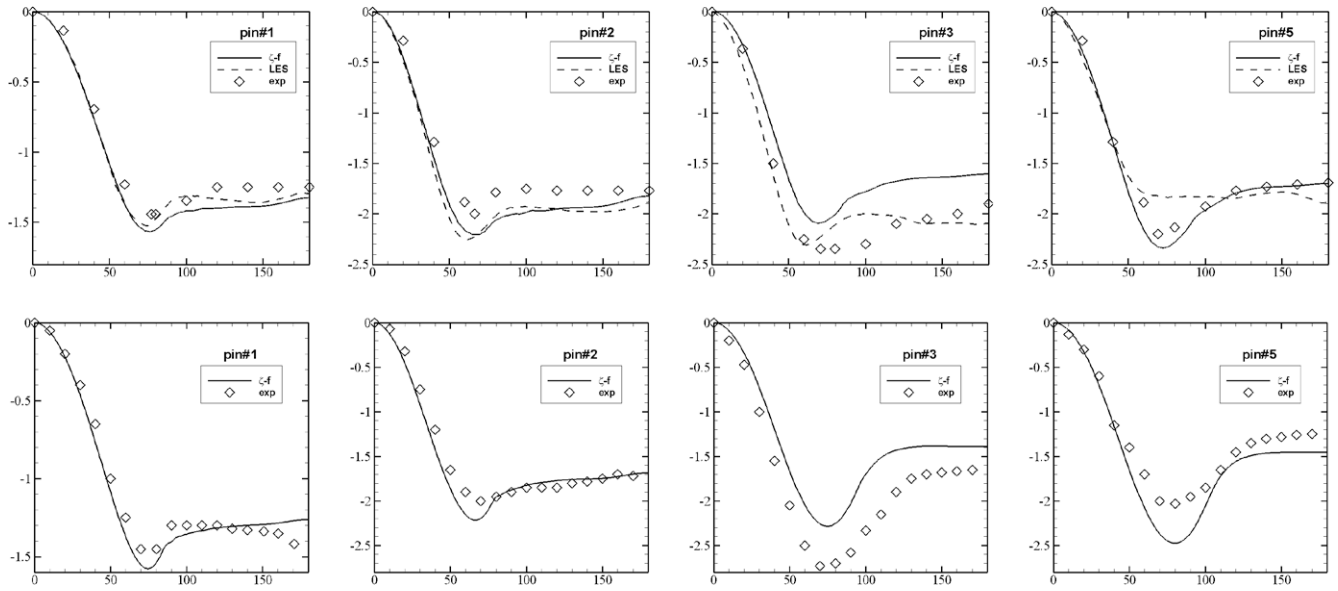

Fig. 8. Distribution of pressure coefficient around pins (lines C, Fig. 2). Top: Re = 10 000; bottom: Re = 30 000.

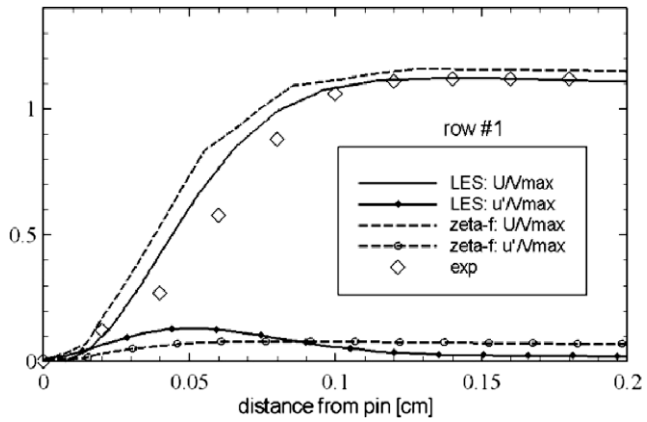

Fig. 9. A blow-up of the velocity distribution close to the pin surface at 90° of pin 1, Re = 10 000.

and URANS velocity profiles should have a small negative value corresponding to a very thin recirculation. Arguably, because hot wire is insensitive to the flow direction, and the Thwaithe's method may not be sufficiently precise, we suspect that the accurate location of the experimental separation is not very certain. On the other hand, computational prediction of the separation location is also sensitive to the local mesh resolution. Thus, the evaluation of friction velocity around separation is prone to large uncertainties and the use of any velocity law that is strictly valid for attached equilibrium wall flows as a basis for its evaluation, is not very reliable. Nevertheless, a comparison of the computed and experimental velocity profiles in wall coordinates depicted in Fig. 10 shows excellent agreement for the third and fifth row for Re = 30 000, both results showing surprisingly even a small portion close to the semi-logarithmic behaviour. Note that the recirculation bubble is so thin that it is not visible (the first computational grid centre is at y^+ about 3–4). Admittedly, the friction velocity u_τ has been tuned (decreased by about 50% from the computed values) to get the best fit of the viscous layer (i.e. $y^+ < 8$). Nevertheless, the excellent agreement indicates that the predictions of the near-wall region – even very close to separation point – is quite satisfactory. Admittedly, for Re = 10 000, the agreement is less convincing (not shown), partially because the recirculation bubble seems to be relatively thicker.

4.2. Flow pattern and its dynamics

As show in Fig. 4, the instantaneous pattern of the vortical structures resolved by LES is much more versatile in sizes and shapes than in URANS. Moreover, apart from the first pin, LES shows no distinct regular cylindrical (almost two-dimensional) shed vortices noticeable in URANS. The key question is how important is to resolve a broad spectrum of large-scale eddy structure for reproducing the mean flow parameters of industrial interest. In order to get a closer insight we compare first the instantaneous and time-averaged streamline patterns, projected in a plane close to the bottom endwall ($z/h = 0.05$), Fig. 11, and at the midplane halfway between the endwalls ($z/h = 0.5$), Fig. 12. Of course, for endwall heat transfer, the flow structure close to the wall is more relevant, but it will also depend on the flow feature in the central region. As expected (and inferred from Fig. 4) the instantaneous streamline patterns generated by LES and URANS in both planes are very different, especially in the near-wall plane. Several notable differences can be identified in Fig. 11:

- In contrast to a very stochastic LES pattern with a strong unsteadiness noticeable in the whole matrix starting with the very first pin, the URANS shows visible unsteadiness and asymmetry of the wake region only after the third or fourth row for both Re; obviously the vortex shedding from the first two rows is insufficient to create bulk unsteadiness and it takes cumulative forcing of several rows to generate sufficiently strong flow instability to produce periodicity in vortex shedding.
- The URANS predicted recirculation regions in the wakes of all pins are much longer and broader than in LES, and this feature extends throughout the whole matrix; moreover, unlike in LES, all recirculation bubbles are similar in size.
- Unlike in LES, where the vortex shedding shows a strong periodicity at all pins, with separation detected over a broad range of angles, approximately 80–150°, the URANS separation at all pins occur around 85 ± 15°.

The time-averaged patterns reflect the above instantaneous features, as shown in Fig. 11. The similarity between URANS and LES is noted only for the first pin where the flow is almost laminar around the complete pin except for a small turbulence indicated in a narrow wake region. Similar conclusions can be drawn for the instantaneous streamline fields in the midplane halfway between endwalls, except that LES shows more vigorous activities as compared with the near-wall plane. However, at the higher Re unsteadiness starts earlier, at around third pin and the subsequent pattern are more similar in between than in for Re = 10 000, Fig. 12.

A blow-up of local instantaneous streamlines around selected pins at the lower Re number is illustrated in Fig. 13 showing clearly that for the midplane the separation on all pins occurs at around

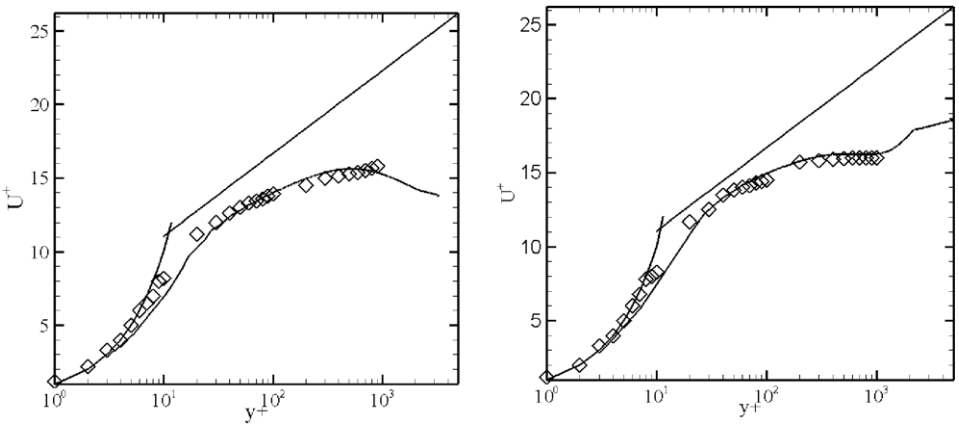

Fig. 10. Velocity profiles at 90° from the impingement for third and fifth row in wall units, ζ-f computations, Re = 30 000.

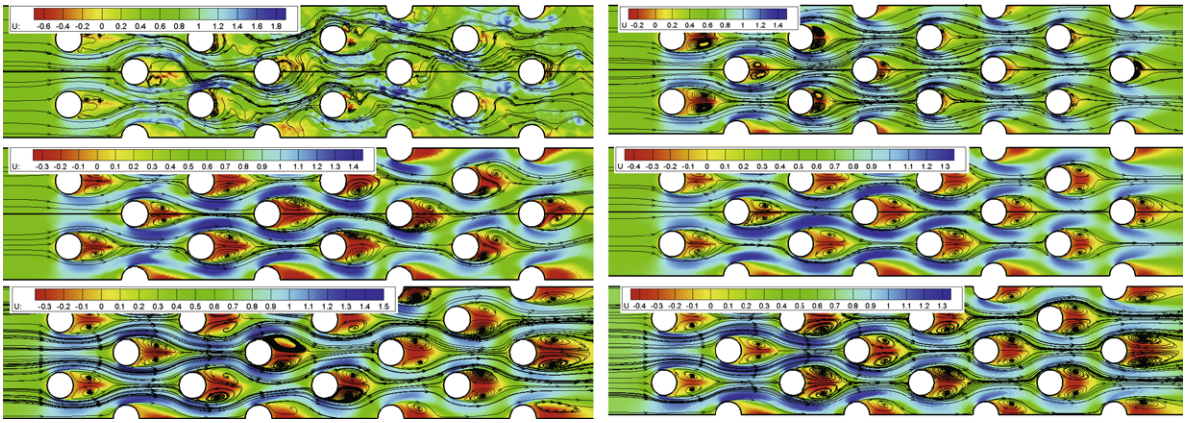

Fig. 11. Streamlines and velocity field (colour bar) in a plane near the bottom endwall (5% of the pin height). Left: instantaneous snapshots; right time-averaged field. Top: LES at Re = 10 000, middle: URANS ζ-f Re = 10 000, bottom: URANS ζ-f Re = 30 000.

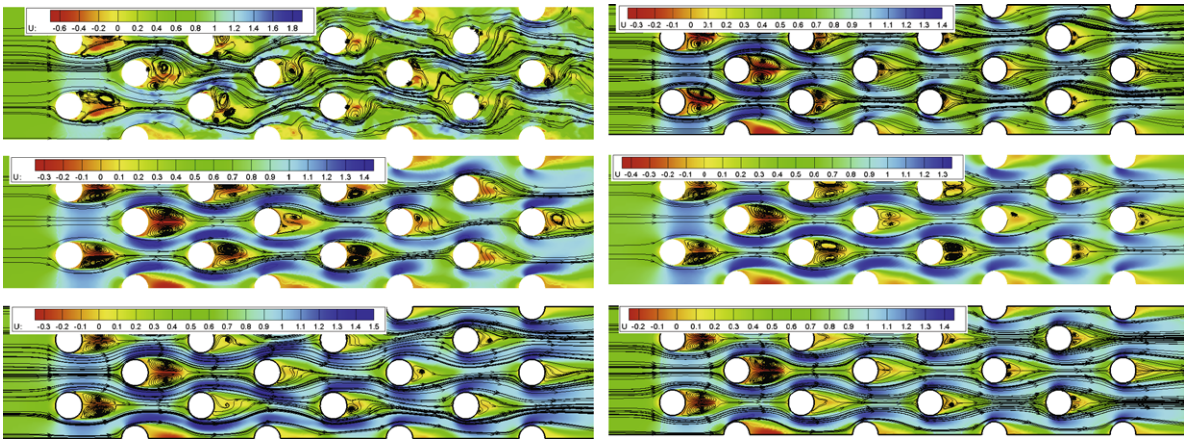

Fig. 12. Streamlines and velocity field (colour bar) in the midplane (50% of the pin height). Left: instantaneous snapshots; right: time-averaged field. Top: LES at Re = 10 000, middle: URANS ζ-f Re = 10 000, bottom: URANS ζ-f Re = 30 000.

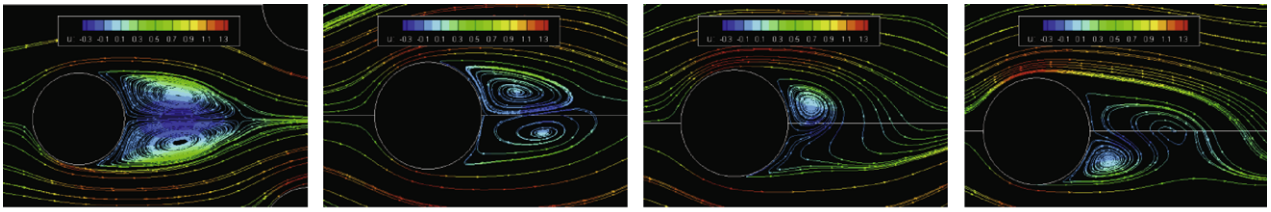

Fig. 13. A blow-up of instantaneous streamlines in midplane after selected pins, illustrating distinct periodic vortex shedding only after fourth row, URANS, Re = 10 000.

90°, indicating subcritical vortex shedding regime. Surprisingly, however, here the time-averaged URANS field shows closer agreement with LES: the recirculating wake regions in URANS are still longer than LES, but the difference is somewhat smaller than in the near-wall plane. This leads to the conclusion that the effect of endwalls on suppression of unsteadiness is differently reproduced by URANS and LES.

While URANS shows little sensitivity to the separation instabilities at first three rows, a sequence of periodic forcing from pins seems to build up, generating eventually strong periodicity in the aft section of the passage with a notable flow flapping after the last pin array. This is illustrated in Fig. 14 by a sequence of selected streamlines at several characteristic instants of a cycle. The flow pattern around the first three pins show very little difference, with the streamline patterns almost symmetric, though some differences can be detected in blown up figures. The main asymmetry appears behind the fourth row and the subsequent pins show a regular oscillatory vortex shedding pattern. This periodicity extends well downstream from the last row, manifested in visible flow flapping in the exit region of the passage. At Re = 30 000, the exiting flow show a more steady pattern with almost no flapping behind the pin matrix.

A better indication of the intensity of the periodic vortex shedding behind the first four rows is illustrated by histograms

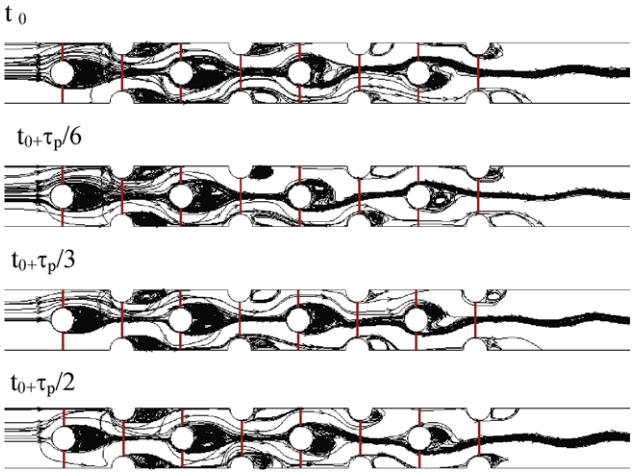

Fig. 14. A sequence of snapshot of streamlines at the midplane within a characteristic cycle (URANS, Re = 10 000).

of the velocity monitored at the point P located close to each pin in one side of the wake, Fig. 15. While the signals after the third and fourth row show clear periodicity with an amplitude of about 50% of the mean velocity (i.e. ±0.5–0.7 m/s) for Re = 10 000, on the same scale the signals behind the first and second pin show hardly any oscillations. Only a large blow-up reveals that both signals are also periodic, though bimodal, but with about two orders of magnitude smaller amplitudes, roughly only 4 mm/s. At Re = 30 000, the amplitudes for all three pins are of the same order of magnitude, as shown in Fig. 15 right, though their relative values for the third pins are smaller than for Re = 10 000.

It is recalled that on the first pin row we see the classic laminar separation on the top of the pins. Experimental velocity monitoring (with a hot wire) at 90° at several points very close to the pin wall, as shown above, confirm that separation is intermittent around this point, as indicated by a significant amplitude of the velocity. Intermittency has also been detected by LES, but URANS failed to reproduce this feature. However, as discussed above, the monitoring at point P behind the separation point and at other larger distance from the pin, the URANS detected regular bimodal periodic pattern of vortex shedding indicate that the separation point is also not fixed by oscillates, though with the amplitudes much smaller than in the experiment.

4.3. Thermal field and heat transfer

We move now to consider the thermal field and heat transfer, the latter being the primary goal of this and related experimental studies used here for comparison. The thermal field was computed by solving the non-dimensional URANS energy equation in term of temperature in parallel with the momentum, continuity and turbulence-model equations. Since no precise thermal boundary conditions are cited in the available literature, we performed computations using either constant wall heat flux or constant wall temperature, both worked out from the average Nusselt number Nu = 54.1 and Nu = 111.5 for the two Reynolds number, reported by experiments (Ames et al., 2007). In both cases, as expected, the same average Nusselt number was obtained, but, of course, the temperature fields are different. We show here results obtained with a constant wall temperature.

Fig. 16 shows a URANS snapshot of the temperature field in the near-wall plane at $z/h = 0.05$. Despite the fact that the imposed wall temperature was constant, significant non-uniformity of the temperature in Fig. 16 and its development along the flow due to continuous heating shows clearly the effect of vortical structures on the thermal field and heat transfer intensity. Strong heat transfer is noticeable under the horse-shoe vortex in particular in front of the first and the few subsequent pins. In contrast, the fluid trapped in the recirculation zones behind the pins show very weak capability of removing heat resulting in high local temperatures. Further downstream the temperature field becomes gradually more uniform due to increasing turbulence level and more efficient mixing.

The evolution of the fluid thermal boundary layer at the bottom endwall throughout the whole solution domain for Re = 30 000 is illustrated in Fig. 17, by showing the temperature field and streamline projections in the vertical midplane cut through the central pin array, and flow-normal cutplanes between the pins in the same

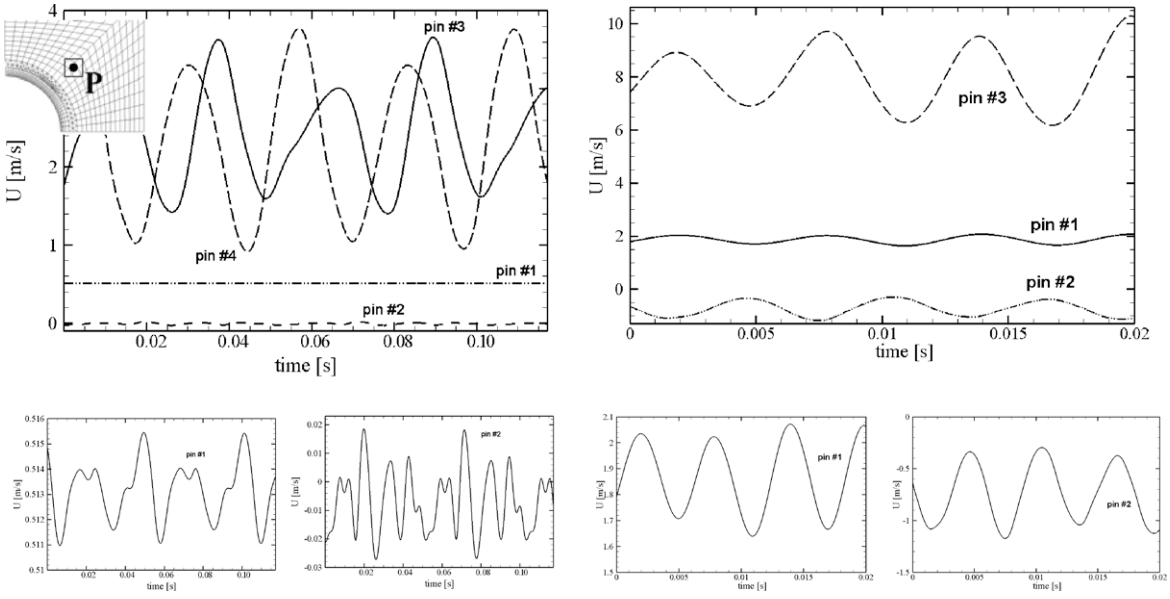

Fig. 15. Velocity monitoring at point P (see insert) behind first 4 pins (top-left) for Re = 10 000 and behind the first 3 pins (top-right) for Re = 30 000. Blow-up of signals behind pin 1 and 2 (bottom).

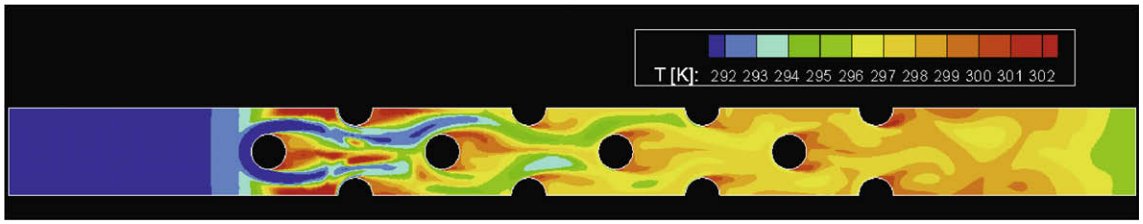

Fig. 16. A snapshot of instantaneous temperature in a plane near the bottom endwall (5% of the pin height), URANS ζ-f, Re = 10 000 (note: wall temperature is constant, T_w = 316 K).

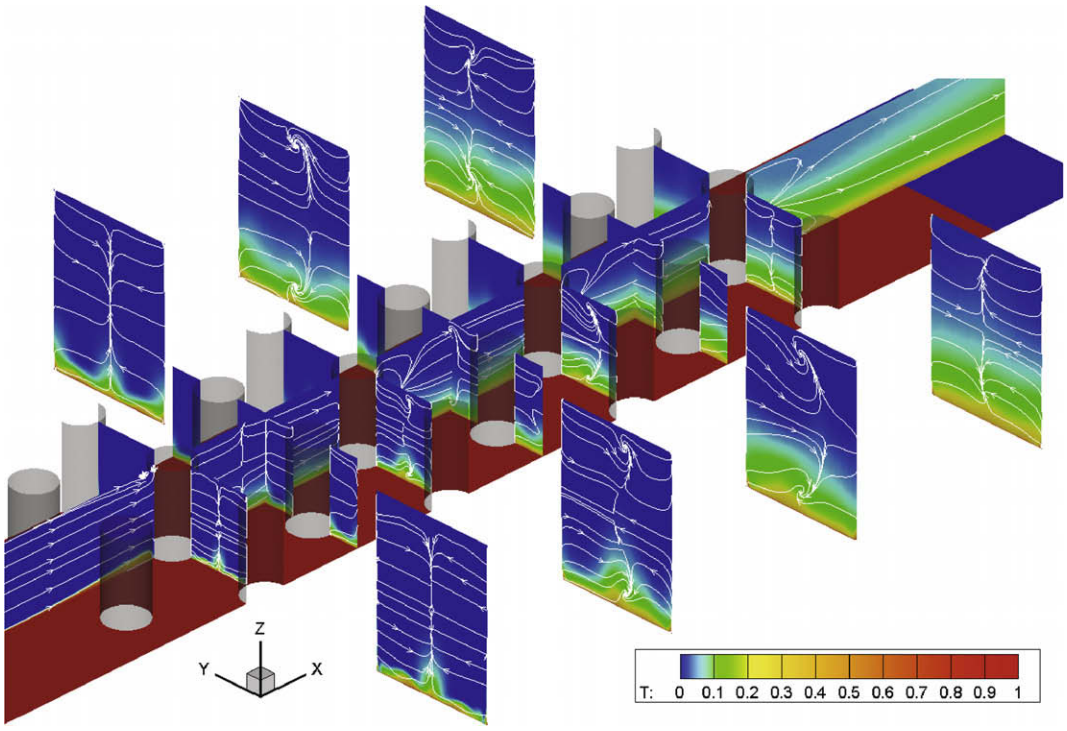

Fig. 17. A snapshot of the development of the thermal boundary layer on the bottom endwall. The thermal plumes indicated in different cross-sections show a close congruence with the streamline pattern projected on the cutplanes.

rows. The streamline patterns show the notable lateral and vertical movement i.e. lateral and vertical components of the three-dimensional velocity field, responsible for heat removal both from the endwalls and pins towards the interim passages. The conspicuous plume-like formation at the bottom heated wall between the pins, in close congruence with the streamline pattern, illustrate the main cause of non-uniformities especially in the upstream portion of the pin passage, with two dips corresponding to more intensive cooling by the tails of horse-shoe vortices. This figure also illustrates the mechanism of heat removal in these regions, which can be credited with a substantial contribution of heat transfer enhancement as compared with a flat wall without pins. Elevated temperature appears behind each pin due to flow recirculation and heat accumulation in the wakes. This non-uniformity gradually levels up downstream.

The above streamlines and temperature patterns are reflected in the instantaneous and time-averaged Nusselt number distributions, shown in Figs. 18 and 19 for the two Re numbers, together with the experimental results. For better comparison, the results are shown separately for the first and second four pins, with different colour/grey-scale bars for each set to enhance the contrast. The colour bars are matched as closely as possible to that in the experiments. Both the instantaneous and mean URANS distributions show very similar pattern. Around the first two pin rows, the patterns are almost identical, while further downstream the instantaneous pattern shows a similar but asymmetric pattern, corresponding to an instant within the flapping cycle. A characteristic feature of URANS results is a larger non-uniformity of Nusselt number in the region around the first four rows, with marked elongated regions between the pins where Nusselt number shows very low values. These elongated blue stripes correspond to regions between the tails of horse-shoe vortices where not much activity is captured by URANS. Here a major difference appears between URANS and LES (not shown here), the latter showing more uniformity in the Nusselt distribution despite very non-uniform instantaneous field. In the aft portion the URANS Nusselt number is also more uniform and not much different from the LES results. In general there is a reasonable agreement in the Nu-contours obtained by experiments, especially in the aft portion of the passage as from the fourth row, except in the central region between the pins where experiments show more uniformity.

It is interesting to note that the time-averaged Nusselt number for the whole heated endwall obtained by URANS is 46, whereas LES with both 2 and 5.5 mill grid cells gives 44. This close agree-

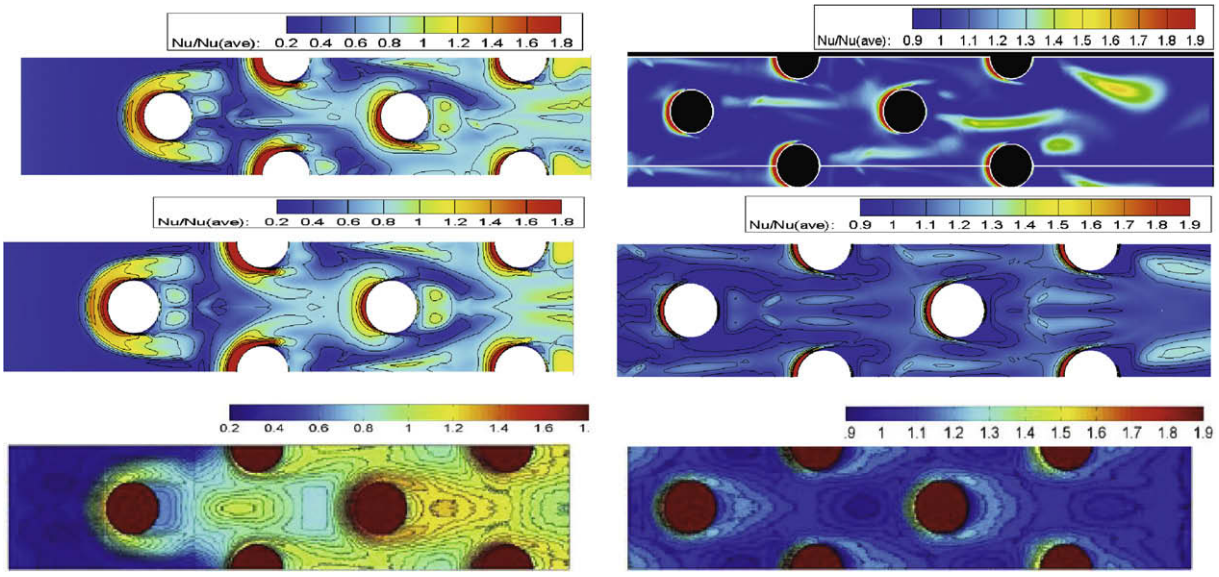

Fig. 18. Nusselt number normalised with $Nu_{ave}(Nu/Nu_{ave})$ on the endwall: Top row: instantaneous snapshots; central row: time-averaged, bottom row: experiments (Re = 10 000).

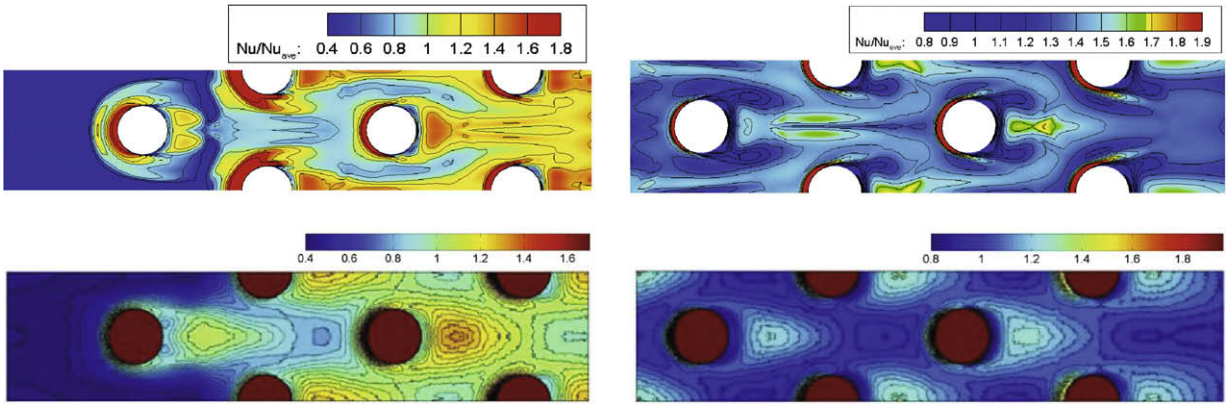

Fig. 19. Nusselt number normalised with $Nu_{ave}(Nu/Nu_{ave})$ on the endwall: Top row: instantaneous snapshots; central row: time-averaged, bottom row: experiments (Re = 30 000).

ment between URANS and LES is surprising in view of substantial differences in the captured flow patterns and local Nusselt number distributions obtained by the two simulation approaches. However, both results fall short by about 20% of the experimental value is 54. While the departure of the URANS results could be attributed to inadequacy of the model for capturing the unsteady flow dynamics and the consequent heat transfer, the LES results, especially on the finer grid and using the dynamic Smagorinsky model are believed to be sufficiently accurate. Assuming that the measurements are reliable and accurate, it seems more likely that the discrepancy between simulations and experiments originates from a mismatch of the inflow conditions. Both in URANS and LES we assumed almost laminar inflow, what may not mimic properly the experimental conditions, with presumably higher turbulence level in the boundary layer along the endwalls. Another cause of discrepancy could be attributed at the effects of radiation, especially at the lower Re number. Radiation heat transfer, not accounted for in the computations, could have been significant in the experiment and although it was claimed to have been accounted for in processing the measured data, it poses some uncertainly. At higher Re number the effect of radiation should be smaller. This is in part substantiated by the URANS results which gave Nusselt number of 122.3, compared to the experimental value of 111.5. The agreement is better than for Re = 10 000, but the computed Nu is now larger than the experimental one. No LES for this Re number is yet available and we suspect that the discrepancy may at least in part be attributed to the RANS model and, perhaps, insufficient grid resolution near

Table 2
Comparison of some computed parameters with experiments and LES

$Re = \frac{DV_{max}}{\nu}$	Strouhal number (pin #1)			Angle of separation in deg. (pin #1)		Averaged endwall Nusselt number		
	Exp.	LES	URANS	Exp.	URANS	Exp.	LES	URANS
10 000	0.234	0.24	0.240	83	85	54.1	44.3	46.2
30 000	0.209	–	0.238	82	87	111.5	–	122.3

the wall for this Re number. The above discrepancies, however, do not affect the main conclusions about the performance of URANS model in reproducing reasonably well the overall unsteady dynamics, the mean velocity and thermal fields and the heat transfer in the considered pin matrix.

5. Conclusions

The unsteady computations of a flow through a matrix of round pins in staggered arrangement connecting heated walls of a plane channel as found in internal cooling of gas-turbine blades, have been performed for two Re numbers, 10 000 and 30 000, using the ζ-f elliptic-relaxation model. The results showed that despite the compact pin arrangement and closeness of the end-wall, which suppress natural instabilities, the model can reproduce the bulk unsteady nature of the flow caused by vortex shedding behind the pins arrays, with the frequencies (see Strouhal numbers, Table 2) close to those found by experiments and LES. However, in contrast to LES, the URANS shows some deficiencies in predicting the wakes behind pins, their structure, size and recirculation strength. This is reflected in a mixed success in predicting pressure recovery behind pins and of velocity profiles. The main discrepancy in the flow pattern and the consequent thermal field and heat transfer appears in the inadequacy of the RANS model considered to respond sufficiently to instabilities that appear already at the first pin row, as evidenced by experiments and LES. Although the separation location is well reproduced, Table 2, the amplitudes of the velocity excursions around the separation point (and thus the oscillations of its location) are by an order of magnitude weaker. Only after a sequence of forcing accumulated from vortex shedding in the first two or three rows, the unsteadiness intensity, measured by the amplitude of the periodic velocity signal at a monitoring point, becomes sufficient to excite the periodic shedding akin to that detected by LES. However, this does not appear to be sufficient to generate a range of eddy scales as in LES, resulting in a different overall flow pattern with longer, broader and more alike recirculating bubbles behind all pins. This different flow pattern and intensity of unsteadiness is reflected in heat transfer, resulting in somewhat different distributions of fluid temperature in the near-wall region, and the Nusselt number on the endwalls, Table 2.

It is expected that a more advanced RANS model at the second-moment closure level or a non-linear eddy-viscosity model would capture better the stress anisotropy which would result in improved time-averaged heat transfer distribution on the endwalls. However it is not clear if an advanced RANS model will be more receptive to instabilities and perform better in capturing unsteadiness in the first portion of the pin passage, or the problem lies in general inability of URANS to capture a broader spectrum of complex vortical structures that has been revealed by LES. While smaller structures cannot be expected to influence directly wall heat transfer as compared to large shed vortices with their surface renewal effect on endwalls, it seems likely that capturing a broader eddy spectrum is important for reproduction accurately the separation incipience, turbulence transition and the consequent wake length and recirculation strength especially at the first row washed by predominantly non-turbulent incoming fluid. Surprisingly, despite notable difference in the flow pattern and unsteadiness intensity, the URANS model returned the averaged (in time and over the surface) Nusselt number very close to that obtained from LES. Both are, however, by 20% lower than the experimental value, indicating at possible mismatching of the experimental conditions and the effect of radiation neglected in the computations. For the higher Reynolds number (for which no LES are available), URANS results come closer to the experiments. Better agreement could be attributed to less effect from the intrinsic weaknesses in reproducing laminar-to-turbulent transition, smaller effects of radiation and of possible mismatch of the imposed inflow conditions.

Acknowledgement

K. Hanjalić acknowledges the award of an EU Marie Curie Chair at DMA, Sapienza Università di Roma.

References

Ames, F.E., Dvorak, L.A., 2006. Turbulent transport in pin-fin arrays: experimental data and predictions. ASME J. of Turbomachinery 128, 71–81.

Ames, F.E., Dvorak, L.A., Morrow, M.J., 2005. Turbulent augmentation of internal convection over pins in staggered pin-fin arrays. ASME J. of Turbomachinery 127, 183–190.

Ames, F.E., Nordquist, C.A., Dvorak L.A., Endwall heat transfer measurements in a staggered pin-fin array with an adiabatic pin. In: Proc. GT2007 ASME Turbo Expo 2007: May 14–17, Montreal, Canada.

Basara, B., 2009. A nonlinear eddy-viscosity model based on an elliptic relaxation approach. Fluid Dyn. Res. 41, 012403 (21pp).

Benhamadouche, S., Laurence, D., 2003. LES, coarse LES, and transient RANS comparisons on the flow across a tube bundle. International Journal of Heat and Fluid Flow 24, 470–479.

Borello, D., Hanjalić, K., Rispoli, F., 2007. Computation of tip leakage flows in a linear compressor cascade with second moment closure. International Journal for Heat and Fluid Flow 28 (4), 587–601.

Borello, D., Delibra, G., Hanjalić, K., Rispoli, F., U-RANS and Hybrid LES/RANS computations of tip-leakage and secondary flows in axial compressor cascade. In: Eighth European Turbomachinery Conference, 23–27 March 2009, Graz, Austria.

Delibra, G., Borello, D., Hanjalić, K., Rispoli, F., LES of flow and heat transfer in a channel with a staggered cylindrical pin matrix. In: ERCOFTAC Workshop on Direct and Large-eddy Simulations, vol. 7, September 8–10 2008, Trieste, Italy.

Durbin, P., 1991. Near-wall turbulence closure modelling without 'damping functions'. Theoret. Comput. Fluid Dyn. 3, 1–13.

Durbin, P., 1995. Separated flow computations with the k–ε–v^2 model. AIAA Journal 33, 659–664.

Dvorak, L., 2004. Turbulent augmentation of heat transfer off pin and endwall surfaces in a staggered pin fin array. M.Sc. Thesis, Grand Forks, North Dakota, December 2004.

Frolich, J., Von Terzi, D., 2008. Hybrid LES/RANS methods fort he simulation of turbulent flows. Progress in Aerospace Sciences 44, 349–377.

Hanjalić, K., 2005. Will RANS survive LES: a view of perspectives. ASME J. Fluids Eng. 127, 831–839.

Hanjalić, K., Kenjereš, S., 2001. "TRANS" simulation of deterministic eddy structure in flows driven by thermal buoyancy an Lorentz force. Flow, Turbulence & Combustion 66, 427–451.

Hanjalić, K., Kenjeres, S., 2006. RANS-based VLES of thermal and magnetic convection at extreme conditions. ASME J. Appl. Mechanics 73 (3), 430–440.

Hanjalić, K., Popovac, M., Hadziabdić, M., 2004. A robust near-wall elliptic-relaxation eddy viscosity turbulence model for CFD. International Journal of Heat and Fluid Flow 25 (6), 1047–1051.

Hanjalić, K., Laurence, D., Popovac, M., Uribe, J.C.M., 2005, v^2/k-f turbulence model and its application to forced and natural convection. In: Sixth Int. Sympos. Engineering Turbulence Modelling and Measurements, May 23–25, 20005, Sardinia, Italy.

Kays, W.M., Crawford, M.E., 1993. Convective Heat and Mass Transfer, third ed. McGrew-Hill, New York.

Krajnović, S., Hemida, H., Basara, B., Schneider, J., Optimization of the aerodynamic performance of vehicles using the ζ-f turbulence model and response surface models. In: Robust Design Through Simulation (submitted), Paris La Défense-Pôle Léonard de Vinci, Paris, France, October 16, 2008.

Metzger, D.E., Shepard, W.B., Haley, S.W., 1986. Row Resolved Heat Transfer Variations in Pin Fin Arrays Including Effects of Non-Uniform Arrays and Flow Convergence. ASME Paper No. 86-GT-132.

Ničeno, B., Hanjalić, K., 2005. Unstructured large-eddy- and conjugate heat transfer simulations of wall-bounded flows. In: Faghri, M., Sunden, B. (Eds.), Modeling and Simulation of Turbulent Heat Transfer (Chapter 2), Developments in Heat Transfer Series. WIT Press, pp. 35–73.

Rodi, W., 1993. On the simulation of turbulent flow past bluff bodies. J. Wind Eng. Ind. Aerodyn. 46–47, 3–19.

Rodi, W., Ferziger, J.H., Breuer, M., Pourquiè, M., 1997. Status of large eddy simulation: result of a workshop. Journal of Fluids Engineering 119, 248–262.

Tatschl, R., Basara, B., Schneider, J., Hanjalić, K. Popovac, M., Brohmer, A., Mehring, J., Advanced turbulent heat transfer modeling for IC-engine applications using AVL FIRE. In: International Multidimensional Engine Modeling User's Group Meeting, April 2, 2006, Detroit, MI.

Watterson, J.K., Dawes, W.N., Savill, A.M., White, A.J., 1999. Predicting turbulent flow in a staggered tube bundle. International Journal of Heat and Fluid Flow 20, 581–591.